Probing the average size of self-assembled metal nanoparticles using x-ray standing waves

M. K. Tiwari,[1,2] K. J. S. Sawhney,[1] Tien-Lin Lee,[1] S. G. Alcock,[1] and G. S. Lodha[2]
[1]*Diamond Light Source Ltd., Harwell Science and Innovation Campus, Didcot, Oxfordshire OX11 0DE, United Kingdom*
[2]*Indus Synchrotron Utilization Division, Raja Ramanna Centre for Advanced Technology, Indore 452013, India*
(Received 7 April 2009; revised manuscript received 3 July 2009; published 30 July 2009)

We report application of x-ray standing-wave field for characterization of average vertical size of metal nanoparticles dispersed on a substrate surface with accuracies better than 1 nm. This method is applied to analyze the distribution of Fe, Co, and Au nanoparticles on Si substrate and W/C multilayer substrates. Results demonstrate that the method is a valuable tool to evaluate the surface morphology of nanoparticles over a large surface area. Unlike conventional probes such as atomic force microscopy or microinterferometry, the present method provides element-specific analysis. It also has the advantage of being able to examine nanoparticles in a liquid medium, or buried inside a coating layer. We anticipate that the proposed method has great potential to infer the internal structure of nanoparticles.

DOI: 10.1103/PhysRevB.80.035434 PACS number(s): 61.46.−w, 68.49.Uv, 78.70.En

I. INTRODUCTION

Dispersion of metal nanoparticles on flat surfaces has attracted considerable interest in many nanotechnology, biotechnology, and semiconductor quantum dot applications.[1–3] Such patterned nanostructures are of great importance in fabricating novel electronic, magnetic, and photonic devices.[4–6] In particular, molecular printing of nanoparticles is highlighted as a method for creating an organized precursor structure on a substrate surface for locating nanowires and carbon nanotubes. The nature of self-assembly of nanoparticles on any flat surface is often inspired by ordering kinetics and nanoparticle's dynamics, irrespective of whether the distribution thus formed is a monodispersion or a complex agglomerate of nanoparticles, which is determined by the minimum free energy in equilibrium conditions. Scanning electron microscopy (SEM) and atomic force microscopy (AFM) are the most commonly used techniques for visualization of distribution of nanoparticles on substrate surfaces. The information of average particle size is determined by recording several images at various locations of the specimen, which is often time consuming. These techniques, moreover, do not provide any information about the physical and chemical state of the nanoparticles and their locations with respect to the substrate surface. Adequate characterization of nanoparticle's distribution on flat surfaces is important in many applications. This type of analysis often appears to be very challenging and sometimes requires complementary methods to infer details of the surface morphology and chemical compositions of the nanoparticles.

X-ray standing-wave (XSW) fields generated by mirror surfaces under total reflection conditions or by synthetic multilayer structures under strong Bragg reflection conditions have been extensively exploited in surface condensed-matter physics for the characterization of heavy ions deposited on the surfaces of organic monolayers, in polymer films,[7–9] and in thick Langmuir-Blodgett films.[10] In most applications, XSW technique has been used to determine the location $\langle z \rangle$ and the width of distribution $\langle z^2 \rangle^{1/2}$ of the atomic impurities in an overlayer. It has been demonstrated that XSW method can determine these quantities with an accuracy of 1%–2% of the XSW period.[11] So far, structural characterization of metal nanoparticles using XSW method has not been reported in the literature. We show that the XSW technique can be used to determine the vertical sizes of metal nanoparticles on a substrate surface. The method provides a possibility to analyze the internal structure and chemical composition of a nanoparticle. In a previous work,[12] we demonstrated that using the XSW field in a total external reflection condition, it is possible to determine the average vertical size of nanoparticles ranging from 30 to 100 nm and their nature of dispersion over a large surface area on a substrate. It was shown that XSW fluorescence profile of the nanoparticles strongly varies if distribution of the nanoparticles on the substrate surface contains monodispersed particles or agglomerates of the nanoparticles. As will be demonstrated below, this method is, however, limited in application to nanoparticles of size less than 30 nm.

In this paper, we report a methodology for determining the size distribution of nanoparticles smaller than 30 nm. The method uses the XSW fields generated by synthetic multilayer structures under Bragg conditions. Using multilayer structures as a substrate, one has the flexibility of tailoring the XSW period in the range of 3–10 nm by selecting appropriate thicknesses of the high and low Z layers of the multilayer. Moreover, variable-period XSW field can be generated by the multilayer surface below the critical angle, providing the possibility to analyze nanoparticles of sizes ranging from 30 to 100 nm. The applicability of the present method has been demonstrated by numerical simulations and by measurements.

II. EXPERIMENTAL DETAILS

Monodispersed distribution of Fe, Co, and Au nanoparticles on a Si and a W/C synthetic multilayer surface was obtained using the spin coating method. The nanoparticles were first dispersed into toluene solution using ultrasonic dispersion. 1%–3% oleic acid was added to this solution as an antiagglomeration agent. The nanoparticle solution was then directly employed for spin coating. After the coating process, the samples were heated to ∼100 °C for 30 min to

 ©2009 The American Physical Society

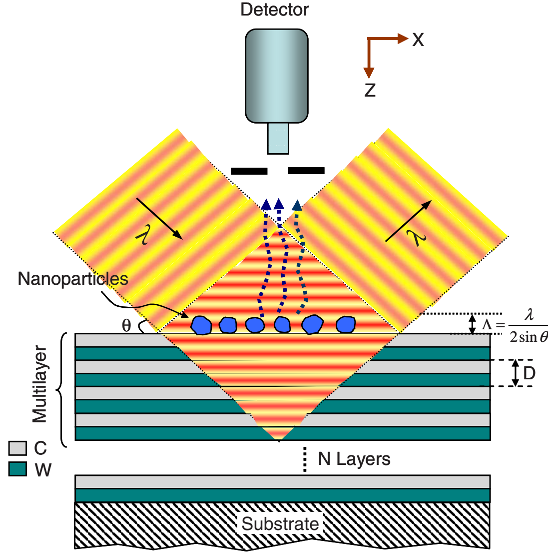

FIG. 1. (Color online) A schematic of x-ray standing-wave-induced fluorescence measurement of metal nanoparticles deposited on top of a multilayer surface.

remove the organic components from the nanoparticle films. This procedure produced uniform distributions of the metal nanoparticles over large surface areas of the substrates. The uniformity of the distributions was confirmed by atomic force microscopy, scanning electron microscopy (SEM, Philips XL30 LEG), and microinterferometric measurements. An AFM system (Danish Micro Engineering Ltd) operating in ac (intermittent contact) mode was employed to study the surface topography of the samples over regions of $\sim 2\ \mu$m $\times 2\ \mu$m. Different regions of the sample surfaces were investigated using computer-controlled sample translation stages. For microinterferometer measurements, a MicroXAM (ADE Phase Shift/KLA Tencor) instrument operating in phase-shifting interferometric PSI mode in conjunction with a 50X Mirau objective lens was employed. XSW measurements were carried out at the B16 Test beamline at Diamond Light Source.[13] Monochromatic x rays of 8 and 12 keV from a Si(111) double-crystal monochromator were used to excite the fluorescent x rays from the nanoparticle samples at grazing incidence angles. As illustrated schematically in Fig. 1, fluorescent x rays emitted from the metal nanoparticles were detected by a vortex spectroscopy detector placed normal to the sample surface. The emitted x rays were measured through a 2-mm Al collimator to maintain a constant solid angle of detection at various incident angles. An avalanche photodiode detector capable of measuring very high count rates and having a large dynamic range was employed to record the intensity of the reflected x rays.

III. THEORETICAL DETAILS

The normalized x-ray field intensity $I_j\ (\theta,Z)$ in layer j of a multilayer structure at depth Z (measured from the interface above) is given by[14]

$$I_j(\theta,Z) = \frac{|E_j^i + E_j^r|^2}{|E_j^i|^2} = \left\{ \exp(-2k''_{j,z} \times Z) + \left|\frac{E_j^r}{E_j^i}\right|^2 \exp(2k''_{j,z} \times Z) + 2\left|\frac{E_j^r}{E_j^i}\right| \cos[\nu(\theta) - 2k'_{j,z} \times Z] \right\}, \tag{1}$$

where E_j^i and E_j^r are the incident and reflected field amplitudes, respectively, at the top of layer j and $\nu(\theta)$ is the phase of the E-field ratio E_j^i/E_j^r.[15] $k'_{j,z}$ and $k''_{j,z}$, respectively, represent the real and imaginary parts of the z component of the incident wave vector. The average x-ray fluorescence intensity emitted from the metal nanoparticles distributed on a multilayer surface can be evaluated by

$$I_f(\theta) \propto \int_0^d I_0(\theta,z) \times f(z) \times \exp\left[-\left(\frac{\mu_{E_0}}{\sin\ \theta} + \frac{\mu_E}{\sin\ \phi}\right) \times z\right] dz, \tag{2}$$

where d is the average vertical size of the nanoparticle layer. z is the relative distance measured from the top of the nanoparticle, $f(z)$ is the mass fraction of the nanoparticles at depth z on the substrate surface, and $\int_0^d f(z)dz = 1$. $I_0\ (\theta,z)$ is the XSW field intensity above the multilayer surface. μ_{E0} and μ_E are the x-ray absorption coefficients for the nanoparticle material at the excitation energy E_0 and emission energy E of the detected element. Φ is the takeoff angle of the emitted fluorescent x rays ($\Phi \sim 90^0$). For nanoparticles of spherical shape, the integral of Eq. (2) can be approximated as[12]

$$I_f(\theta) \propto \int_0^{2d/3} I_0(\theta,z) \times \exp\left[-\left(\frac{\mu_{E_0}}{\sin\ \theta} + \frac{\mu_E}{\sin\ \phi}\right) \times z\right] dz. \tag{3}$$

In the derivation of the above equations we have assumed that the nanoparticles are dispersed in the form of a monolayer but are sufficiently apart so as not to form a continuous layer structure. Moreover, we have ignored any perturbation to the XSW field intensity arising from scattering of the incident x rays from the nanoparticle layer. It should be noted that the maximum height that can be expected to have well-defined XSW fields in a triangular region above the multilayer surface, where incident and reflected beam cross each other, depend on the longitudinal or temporal coherence length of the incident radiation.[16] This height typically ranges in few hundreds nanometers (ca. 300–800 nm).

IV. RESULTS AND DISCUSSION

In order to investigate the validity of average size determination of small nanoparticles ($\leq$30 nm) using the multilayer-assisted XSW field [Eq. (3)], we have performed numerical simulations. Figure 2(a) depicts the calculated x-ray field intensity in a W/C multilayer (D=11.5 nm, structure factor=0.348, N=10 layer pairs) and Fig. 2(b) gives the incident angle dependence of the x-ray fluorescence intensity

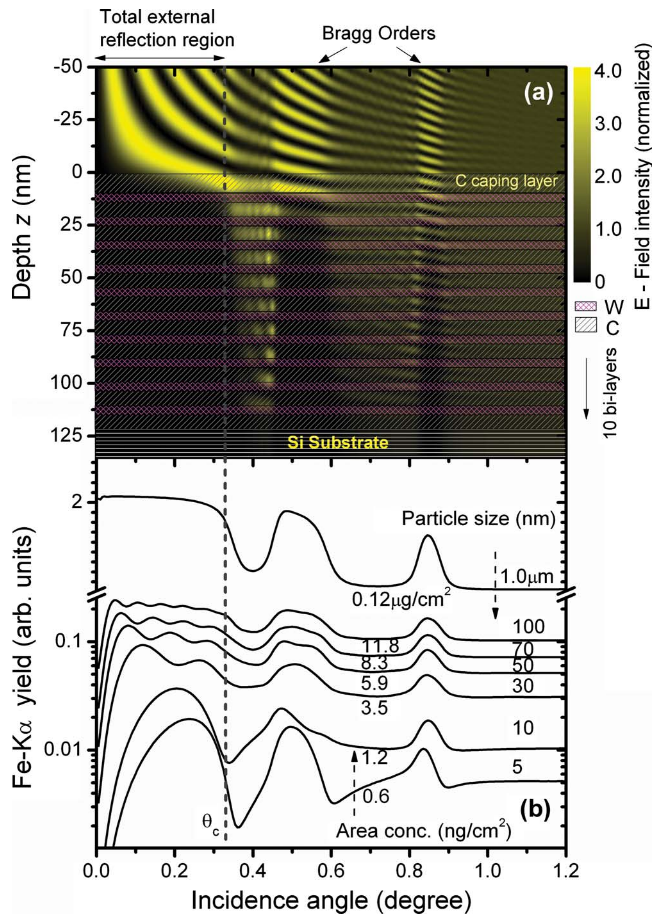

FIG. 2. (Color online) (a) The contour plot of x-ray field intensity distribution in a W/C multilayer structure as a function of incidence angle and the depth z of multilayer medium at x-ray energy of 8.0 keV, (b) Calculated fluorescence profiles of Fe nanoparticles deposited on top of a W/C multilayer, with different particle size distributions and area concentrations. The W/C multilayer employed in the present paper consists of an additional capping layer of carbon of thickness 6 nm, which helps in protecting the degradation of the upper layers of multilayer structure, arising due to oxidation or chemical treatment used in depositing nanoparticles on its surface.

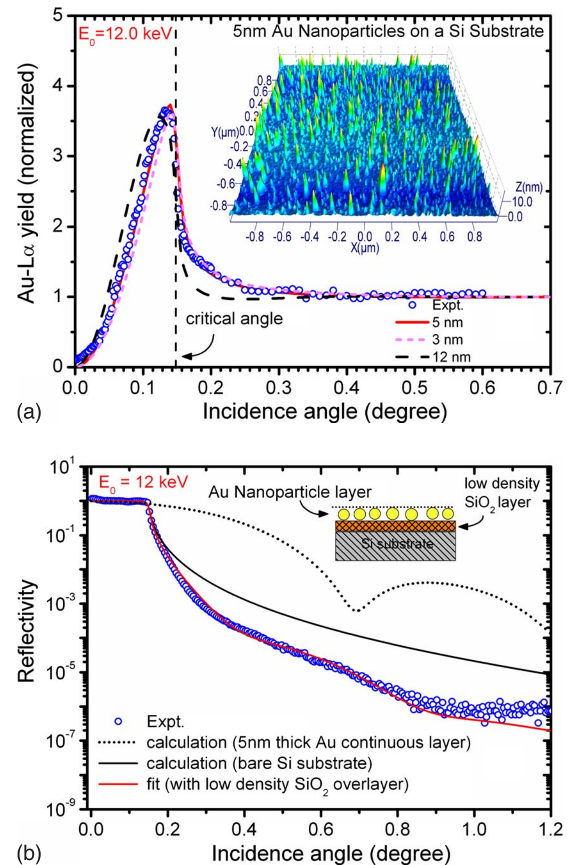

FIG. 3. (Color online) (a) Measured and calculated angle-dependent x-ray fluorescence profiles of Au nanoparticles present on top of Si substrate at x-ray energy of 12.0 keV. The curves of Au Lα fluorescence have been normalized at an incidence angle of 0.6°. (b) Measured and fitted x-ray reflectivity profiles are shown. The insets, respectively, show the AFM image and layer configuration of the distribution of Au nanoparticles on Si substrate.

profile for Fe nanoparticles of different sizes. In the contour plot of x-ray field intensity in Fig. 2(a) it can be seen that XSW fields of various periodicities are produced above the multilayer surface below the critical angle and across the Bragg regions. Figure 2(b) shows that by progressively decreasing the nanoparticle size to 100–30 nm, small modulations in the fluorescence profile appear below the critical angle. As the particle size further reduces, the amplitudes of fluorescence modulations increase toward the highest possible value of four and the modulations across the Bragg regions become more sensitive to the particle size. For particles larger than 100 nm, interference effects vanish and the fluorescence intensity is then simply given by the sum of the contributions of the individual excitations from the incoming and reflected beams. In these calculations, the surface density of the nanoparticles is assumed to vary from 0.12 μg/cm^2 to 0.6 ng/cm^2.

Figure 3 shows the measured x-ray fluorescence yield and reflectivity versus the incident angle for a layer of 5-nm Au nanoparticles on a Si substrate surface. From Fig. 3(a) it can be seen that the fluorescence profile of the Au Lα shows strong peaking behavior in the vicinity of the critical angle of the Si substrate (θ_c=0.148°). This peaking behavior arises from the coincidence of the first XSW antinode with the volume of the nanoparticles. The period of the XSW field under total external reflection condition is given by $\Lambda = \lambda/2 \sin \theta$. As one decreases the incidence angle below θ_c, the XSW antinode moves upward in the air and also the XSW field period expands accordingly. At the critical angle the first XSW antinode lies exactly at the air-substrate interface and the period of the XSW is defined to be the critical period Λ_c,[10] which is inversely proportional to $\sqrt{N_a \times Z_a}$, where N_a and Z_a are the atom density and atomic number, respectively, of the reflecting surface. When the particles are much smaller than Λ_c, which is about 20 nm for Si, the coincidence of the first XSW antinode with the particles can only occur very near the critical angle. Figure 3(a) further shows that the fluorescence profiles appear essentially the same for particles of size <12 nm. Thus, using the long, variable period XSW generated under a total external reflec-

tion condition it is difficult to estimate the average size of small nanoparticles. The inset in Fig. 3(a) shows an AFM measurement for the monodispersed Au nanoparticles. AFM images taken at several locations on the substrate surface gave an average size of 5 ± 1 nm for the Au nanoparticles. The x-ray reflectivity measurement in Fig. 3(b) shows a critical angle, which matches with the critical angle of the bare Si substrate rather than that of a 5-nm-thick continuous Au layer. This confirms that the Au nanoparticles are sparsely distributed on the Si substrate surface. A detailed fit of the x-ray reflectivity profile further reveals the formation of a SiO_2-like low-density layer of ~4.6 nm thickness and ~1.4 nm roughness. This low-density SiO_2 layer is expected to form on the Si substrate surface during the spin coating process.

The measured and fitted angle-dependent x-ray fluorescence profiles for the Fe and Co nanoparticles deposited, respectively, on a Si and a W/C multilayer surfaces are shown in Fig. 4. In Fig. 4(a) the average vertical size of the Fe nanoparticles is determined to be 30 ± 1.5 nm using the variable-period XSW generated by the Si mirror in the total external reflection condition. It can be seen that even if the particle height is larger than Λ_c, one observes only a single period of the modulation in the fluorescence profile, which peaks well below the critical angle. The second period of the modulation is barely visible in the vicinity of the critical angle of the substrate. When these Fe nanoparticles are dispersed on the W/C multilayer surface [Fig. 4(b)], one can see distinctly the second peak in the fluorescence profile below the critical angle of the multilayer substrate ($\theta_c\sim0.345°$). Compared to Fig. 4(a), the observation of two peaks in Fig. 4(b) results from the fact that W/C multilayer has a much smaller Λ_c (~12 nm) than Si substrate, allowing the second XSW antinode to reach the Fe nanoparticles far below the critical angle. For the Co nanoparticles of 6 nm size [Fig. 4(c)], which is about twice the amount smaller than the XSW period (=multilayer D spacing) of the first-order reflection of the multilayer (11.5 nm), the fluorescence profile changes remarkably across the angular range of the first Bragg peak [cf. Figs. 4(b) and 4(c)]. Below the critical angle, because the particle size is smaller than Λ_c of the multilayer surface, one observes a single peak in the fluorescence profile with its intensity maximum close to antinode intensity (~4 times). Figure 4 thus shows that the particle height can strongly influence the modulation in the fluorescence profile either below the critical angle or across the Bragg reflection regions.

The best fit to the data in Fig. 4(b) yields an average vertical size for the Fe nanoparticles on the W/C multilayer surface of 29.0 ± 0.6 nm. Because of the presence of several modulation peaks in the fluorescence profile one obtains greater accuracy in the particle size determination. The SEM measurements (insets in Figs. 4(a) and 4(b)) clearly indicate monodispersion of the Fe nanoparticles on the Si and W/C multilayer substrate surfaces. For the Co nanoparticles the average size is determined by the multilayer-assisted XSW measurement [Fig. 4(c)] to be 6.5 ± 0.5 nm. We could not analyze these particles with SEM because of the spatial resolution limit of the SEM instrument. Using a microinterferometer [inset in Fig. 4(c)] we measure the size of the Co

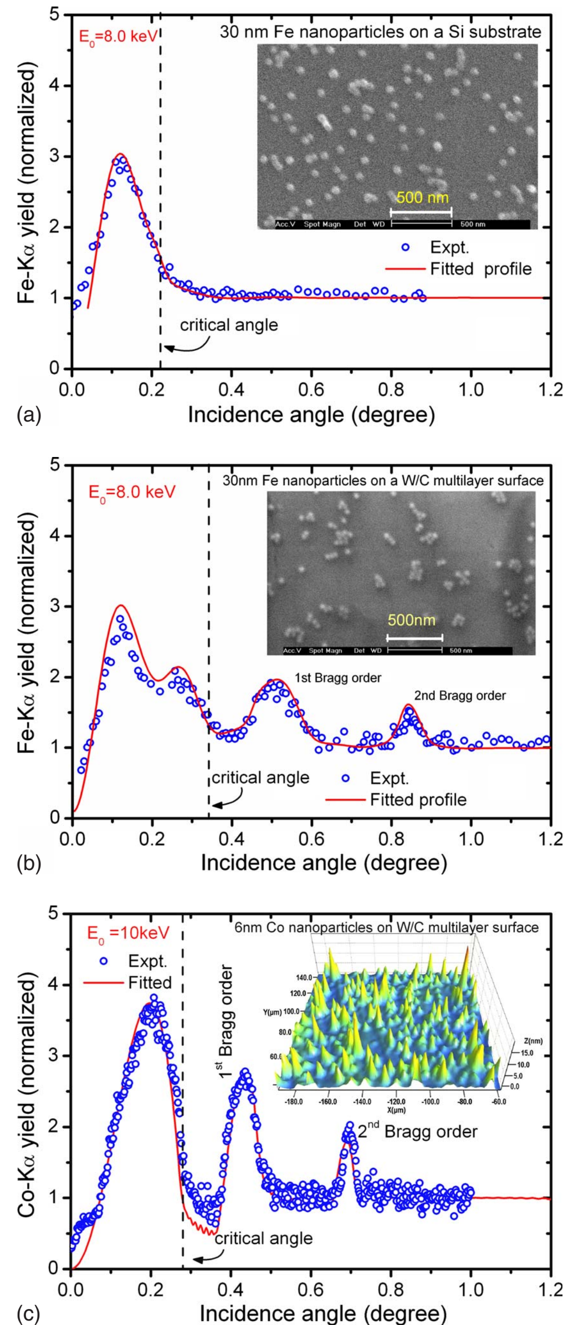

FIG. 4. (Color online) Measured and fitted angle-dependent x-ray fluorescence profiles for Fe and Co nanoparticles at x-ray energies of 8.0 and 10.0 keV. (a) Fe nanoparticles on top of a Si substrate, (b) Fe nanoparticles on top of W/C multilayer mirror (D=11.5 nm, structure factor=0.348, N=10 layer pairs), and (c) Co nanoparticles on top of W/C multilayer. The fluorescence curves have been normalized at the value at high incidence angles (as in Fig. 3). The insets show the SEM and microinterferometer images for Fe and Co nanoparticles.

particles to be 5 ± 2 nm, which matches very well with the values obtained by XSW. Table I summarizes the results of all the measurements. We could not use the W/C multilayer substrate for the characterization of the Au nanoparticles because of the strong overlap of Au Lα with the W L fluorescence lines. To overcome such problems, we plan to use

TABLE I. Determined average vertical sizes for the various metal nanoparticles using XSW, AFM, and microinterferometry techniques.

	Particle size (nm)		
Nanoparticle material	Long period XSW field	Multilayer XSW field	Other methods (AFM and optical interferometer)
Fe	30 ± 1.5 nm	29.0 ± 0.6 nm	31 ± 2 [a]
Co	Not sensitive	6.5 ± 0.5 nm	5.0 ± 2

[a]Reference 12.

multilayer structures comprising of medium Z elements such as Mo/Si or Nb/C, for future studies.

V. CONCLUSIONS

On the basis of the above results, we conclude that the method presented here provides an accurate and fast way to determine the average vertical size of metal nanoparticles dispersed on substrate surfaces. Furthermore, we have shown that the sparsely distributed metal nanoparticles on top of a mirror substrate do not form a continuous layer structure, and instead it only increases the effective surface roughness of the substrate. A single measurement is sufficient to determine the aggregate average size of the nanoparticles over large surface areas, obviating the need to perform several measurements over small regions of the specimen, as is commonly required in more conventional probes. The method, in addition, benefits from all the features of x-ray fluorescence technique. Thus, it would be applicable, with equal ease, for analyzing all kinds of metal and metalloid mixture nanoparticle distribution on a flat surface, for their surface morphologies and chemical compositions. The method does not depend on the crystalline or amorphous nature of the nanoparticles. We predict widespread applications of our method, especially for analyzing nanostructure materials for their structural and electronic properties, if depth-sensitive advantage of x-ray standing-wave method is coupled with other analytical techniques, for example, x-ray photo electron spectroscopy, x-ray diffraction, and auger electron spectroscopy.

ACKNOWLEDGMENTS

This work was carried out with the support of the Diamond Light Source. The authors thank B16 beamline technical staff for their generous assistance and GM Bhalerao for providing Fe nanoparticles.

[1] H. E. Ruda, J. C. Polanyi, J. S. Y. Yang, Z. Wu, U. Philipose, T. Xu, S. Yang, K. L. Kavanagh, J. Q. Liu, L. Yang, Y. Wang, K. Robbie, J. Yang, K. Kaminska, D. G. Cooke, F. A. Hegmann, A. J. Budz, and H. K. Haugen, Nanoscale Res. Lett. **1**, 99 (2006).

[2] S. J. Henley, J. D. Carey, and S. R. P. Silva, Appl. Phys. Lett. **89**, 183120 (2006).

[3] D. C. Sundberg and Y. G. Durant, Polym. React. Eng. **11**, 379 (2003).

[4] J. Shi, S. Gider, K. Babcock, and D. D. Awschalom, Science **271**, 937 (1996).

[5] Z. Y. Zhong, B. Gates, Y. N. Xia, and D. Qin, Langmuir **16**, 10369 (2000).

[6] C. Antoniak, J. Lindner, M. Spasova, D. Sudfeld, M. Acet, M. Farle, K. Fauth, U. Wiedwald, H. G. Boyen, P. Ziemann, F. Wilhelm, A. Rogalev and S. Sun, Phys. Rev. Lett. **97**, 117201 (2006).

[7] R. S. Becker, J. A. Golovchenko, and J. R. Patel, Phys. Rev. Lett. **50**, 153 (1983).

[8] S. Narayanan, D. R. Lee, R. S. Guico, S. K. Sinha, and J. Wang, Phys. Rev. Lett. **94**, 145504 (2005).

[9] D. R. Lee, A. Hagman, X. Li, S. Narayanan, and J. Wang, Appl. Phys. Lett. **88**, 153101 (2006).

[10] M. J. Bedzyk, G. M. Bommarito, and J. S. Schildkraut, Phys. Rev. Lett. **62**, 1376 (1989).

[11] H. D. Abruna, G. M. Bommarito, and D. Acevedo, Science **250**, 69 (1990).

[12] M. K. Tiwari, G. M. Bhalerao, M. Babu, A. K. Sinha, and C. Mukherjee, J. Appl. Phys. **103**, 054311 (2008).

[13] http:// www.diamond.ac.uk / Beamlines / Beamlineplan / B16/ index.htm

[14] D. K. G. de Boer, Phys. Rev. B **44**, 498 (1991).

[15] In the recursion method, for a layered specimen, the incident field E_j^i, and reflected field E_j^r at the top of a jth layer can be obtained from $E_j^r = a_j^2 X_j E_j^i$, and $E_{j+1}^i = \frac{a_j E_j^i t_j}{1+a_{j+1}^2 X_{j+1} r_j}$, where $a_j = \exp(-ik_{j,Z} d_j)$ and $X_j = \frac{(r_j + a_{j+1}^2 X_{j+1})}{1+a_{j+1}^2 X_{j+1} r_j}$. d_j represents thickness of layer j.

[16] T. P. Trainor, A. S. Templeton, G. E. Brown, Jr., and G. A. Parks, Langmuir **18**, 5782 (2002).